Materials Advances

ROYAL SOCIETY OF CHEMISTRY

PAPER

View Article Online
View Journal | View Issue

Cite this: *Mater. Adv.*, 2022, 3, 7579

A tough fluorescent nanocomposite hydrogel probe based on graphene quantum dots for the selective detection of Fe^{3+} ions†

Juan Du, * Wenli Zhu, Xiaohong She, Qiyu Yu, Qiaoling Yang, Huiping Huang, Chihui Tsou and De Guzman Manuel

Herein, poly(acrylamide-*co*-acrylic acid)/GQD (poly(AM-*co*-AA)/GQD) nanocomposite hydrogels were prepared by *in situ* free radical polymerization using graphene quantum dots (GQDs) as a multifunctional crosslinker. The appropriate size and plenty of surface functional groups enabled GQDs to effectively adsorb large amounts of polymer chains and act as a multifunctional crosslinker in gels, thus forming a denser and more uniform crosslinked network in poly(AM-*co*-AA)/GQD nanocomposite hydrogels, and in turn endow the resultant nanocomposite hydrogel with excellent mechanical properties and self-healing properties. Compared to poly(AM-*co*-AA) hydrogels, about a 4.04-fold increase of tensile strength, a 4.51-fold increase of elongation at break and 1.06 times compressive strength compared to those of poly(AM-*co*-AA) hydrogels were achieved when the content of GQDs in poly(AM-*co*-AA)/GQD nanocomposite hydrogels was 1 wt%, suggesting that GQDs could effectively improve the mechanical properties of the hydrogels. Besides, GQDs could give poly(AM-*co*-AA)/GQD nanocomposite hydrogels excellent fluorescence, and a strong blue luminescence emission at a maximal peak at 459 nm when they were excited at 360 nm. Moreover, due to the fluorescence quenching of GQDs, the obtained poly(AM-*co*-AA)/GQD nanocomposite hydrogels were able to sense Fe^{3+} ions. As a result, the nanocomposite hydrogels were selective to Fe^{3+} ions, and the fluorescence intensity linearly responded to the Fe^{3+} ion concentration in the range of 10–160 μmol L^{-1} (R^2 = 0.9686). The fluorescence hydrogel can be used as an effective fluorescent probe for the detection of Fe^{3+} ions in an aqueous solution in the future.

Received 29th May 2022,
Accepted 28th July 2022

DOI: 10.1039/d2ma00605g

rsc.li/materials-advances

Introduction

Fe^{3+} is widely distributed in biological systems and natural environments. It is mainly involved in oxygen transport, DNA synthesis, electron transport and other metabolic processes in the human body.[1–4] However, it is known that iron overload is related to tissue or organ damage associated with diseases such as hepatitis, hemochromatosis, organ dysfunction, and neurodegenerative diseases.[2–6] In addition, the World Health Organization has declared that Fe^{3+} ions in water are an undesirable secondary contaminant, which not only affects the aesthetic appeal of water, but also promotes the growth of iron-oxidizing bacteria (*Gallionella ferruginea*, *Leptothrix ochracea* and *Toxothrix trichogenes*, *etc.*). Therefore, the determination of iron content is essential for the prevention, diagnosis, and treatment of these diseases. Recently, researchers have detected Fe^{3+} ions by atomic adsorption spectroscopy, inductively coupled plasma mass spectrometry, electrochemical methods, chemiluminescence methods, spectrophotometry, colorimetric methods and other methods.[7–12] Different from some of these instrumental techniques requiring sophisticated instrumentation and expensive facilities, fluorescent sensors have been considered as a useful tool to detect Fe^{3+} ions due to their high sensitivity, good selectivity and rapid detection.

Graphene quantum dots (GQDs) are zero-dimensional graphene nanoparticles that retain the highly crystalline structure of single- or few layer graphene. Recently, they have emerged as highly promising nanomaterials for fluorescence-based sensing applications due to their strong quantum confinement and edge effects, high fluorescence quantum yield, easily tunable photoluminescence, stable aqueous dispersion, low toxicity or even non-toxicity, good biocompatibility, tunable band gaps, and easy modification compared with traditional organic fluorescent materials and inorganic quantum dots.[13–17] Many reports

Key Laboratory of Material Corrosion and Protection of Sichuan Province, College of Materials Science and Engineering, Sichuan University of Science and Engineering, Zigong 643000, China. E-mail: dujuan@suse.edu.cn

† Electronic supplementary information (ESI) available: Atomic force microscopy images, 3D topographic map and the height distributions of the synthesized GQDs; Raman spectra of GQDs and poly(AM-*co*-AA)/GQD hydrogels. See DOI: https://doi.org/10.1039/d2ma00605g

indicated that GQDs had absolute selectivity and sensitivity toward some metal ions. Under the action of specific metal ions, GQDs can perform fluorescence quenching, so as to realize the detection of metal ions. Therefore, GQDs are promising fluorescent probes for the detection of Fe^{3+}, Pb^{2+}, Cu^{2+}, Cr^{3+} and other metal ions.[18] However, due to the tendency of aggregation-induced quenching of GQDs in aqueous solution, the actual detection effect is affected. Therefore, it is of great significance to find suitable matrix materials to carry GQDs. One possible approach is to immobilize GQDs in a suitable matrix that retains the properties of GQDs in solutions while still being permeable to the surrounding analytes.

Hydrogels are a kind of soft-wet material composed of large amounts of water and three-dimensional cross-linked polymer networks that can encapsulate foreign molecules or nanoparticles within their spongy structure.[15,19] Recently, hydrogel materials have been widely used in the fields of continuous drug delivery, tissue engineering scaffolds, medical implants, nanocarriers, biosensing, soft actuators, and electronics.[20–24] However, due to their inherent structural heterogeneity and lack of an effective energy dissipation mechanism, most hydrogels have low mechanical strength, which greatly limits their applications. Therefore, it is urgent to design and fabricate mechanically robust hydrogels. To boost their practical potential, various hydrogels with enhanced mechanical properties have been developed recently, such as topological hydrogels, double network hydrogels, nanocomposite hydrogels and macromolecular microsphere composite hydrogels.[25–28] The most notable tough hydrogels are nanocomposite hydrogels. Nanocomposite hydrogels are identified to be a simple tool to enhance the mechanical properties of hydrogels through the addition of reinforcing organic/inorganic fillers such as LAPONITE®, montmorillonite, graphene oxide, TiO_2, SiO_2 and carbon nanotubes.[27,29–35] Functioning as a multifunctional crosslinker, these nanoparticles can associate with the polymer matrix through noncovalent bonding such as hydrogen bonds, electrostatic interactions and coordination bonds.[27,36] When one polymer chain fails under large deformation, severe stress concentration is relaxed by distributing the load to the other polymer chains. Therefore, nanocomposite hydrogels generally possess high tensile strength (up to 1.1 MPa) with high elongation (up to 800%).[32]

Interestingly, this hydrogel is also able to combine the characteristics of nanomaterials and hydrogels together.[27,33,37–46] Inspired by this, we explored the preparation of tough nanocomposite hydrogels using GQDs as a multifunctional crosslinker. The desired hydrogels with high strength and fluorescence performance could be obtained through the combination of GQDs with gel network ingeniously. Moreover, it is of great significance to introduce GQDs with fluorescence characteristics into the porous structure of hydrogels. The porous network of hydrogels allows small molecules and ions to penetrate into the hydrogel's matrix by diffusion, while GQDs with a size comparable to or larger than the pore size of the hydrogels can be captured in the polymer networks. Furthermore, the abundant hydrophilic groups in the hydrogel network can be firmly bonded with carboxyl and hydroxyl groups on the surface of GQDs *via* noncovalent bonds, thus obtaining a tough GQD-based nanocomposite fluorescent hydrogel. When an external force is applied, the GQDs as the stress transfer center can dissipate the external stress effectively, so as to avoid stress concentration and achieve the toughening effect. More importantly, its fluorescence characteristics enable it to satisfy the practical use in fluorescent probes. The immobilization of GQDs in a hydrogel matrix not only makes it possible to detect heavy metals rapidly, but also greatly reduces the influence caused by the analyte that is not related to the analysis results.

In this work, poly(AM-*co*-AA)/GQD nanocomposite fluorescent hydrogels were successfully prepared by *in situ* free radical polymerization of monomer acrylamide (AM) and acrylic acid (AA) in the GQD aqueous dispersion. In this hydrogel, nanosized GQDs interacted with poly(AM-*co*-AA)/GQD chains and formed a tight physical network through hydrogen bonding. Based on the existing high density hydrogel network, the stress could be dissipated effectively through the fracture and recombination of noncovalent bonds during the deformation process. As a result, these poly(AM-*co*-AA)/GQD nanocomposite hydrogels could be stretched over 3437% with a fracture strength as high as 344.22 kPa. Meanwhile, GQDs endowed the nanocomposite hydrogels with good fluorescence characteristics. They could emit strong blue light under 360 nm excitation, and their maximum emission peak was at 459 nm. Moreover, the prepared poly(AM-*co*-AA)/GQD nanocomposite hydrogels could sense Fe^{3+} ions and their fluorescence intensity had a linear response with the concentration of Fe^{3+} ions in the range of 10–160 μmol L^{-1}, and thus can serve as an effective fluorescent probe for the detection of Fe^{3+} ions in aqueous solution.

Experimental

Materials

Citric acid monohydrate, sodium hydroxide (NaOH), zinc(II) nitrate hexahydrate ($Zn(NO_3)_2{\cdot}6H_2O$), lead(II) nitrate ($Pb(NO_3)_2$) and absolute ethyl alcohol were purchased from Chengdu Chron Chemicals Co., Ltd (Chengdu, China). Acrylic acid (AA), nickel(II) nitrate hexahydrate ($Ni(NO_3)_2{\cdot}6H_2O$) and ferric(III) chloride hexahydrate ($FeCl_3{\cdot}6H_2O$) were provided by Aldrich Chemical Co. (Shanghai, China). Acrylamide (AM) was purchased from Tianjin Kemiou Chemical Reagent Co., Ltd (Tianjin, China). Ammonium persulfate (APS), calcium(II) chloride hexahydrate ($CaCl_2{\cdot}6H_2O$) and copper(II) sulfate pentahydrate ($CuSO_4{\cdot}5H_2O$) were supplied by Chengdu Kelong Chemical Reagent Factory (Chengdu, China). *N*,*N*,*N*′,*N*′-tetramethylethylenediamine (TEMED) was purchased from Adamas Reagent, Ltd (Shanghai, China). Magnesium(II) sulfate heptahydrate ($MgSO_4{\cdot}7H_2O$), chromic(III) chloride hexahydrate ($CrCl_3{\cdot}6H_2O$) and barium(II) chloride dehydrate ($BaCl_2{\cdot}2H_2O$) were purchased from Greagent-bate Reagent, Ltd (Shanghai, China). All reagents were of analytical grade and were used as received without further purification. Deionized water was used in all experiments. Salt solutions

of Ba^{2+}, Ca^{2+}, Cr^{3+}, Fe^{3+}, Cu^{2+}, Mg^{2+}, Ni^{2+}, Pb^{2+} and Zn^{2+} were prepared in deionized water with a concentration of 100 μmol L^{-1}.

Synthesis of GQDs

GQDs were prepared by pyrolyzing citric acid according to the procedure reported by Alizadeh *et al.*[47] In a typical procedure, 2.0 g of citric acid was put into a 5.0 mL beaker and heated to 200 °C. After 20 min, the color of the melted product became orange, hinting at the formation of GQDs. Next, the pH value of the obtained orange liquid was adjusted to 7.0 by NaOH solution (10 mg mL^{-1}). Afterward, a certain volume of ethanol was added to the solution above according to the volume ratio of ethanol to solution of 5 : 1 and then stood for 10 min. Subsequently, the solution was transferred to a centrifuge tube and centrifuged at 10 000 RPM for 10 min. The precipitates were GQDs, which were collected and stored away from light.

Preparation of poly(AM-*co*-AA)/GQD nanocomposite hydrogels

Poly(AM-*co*-AA)/GQD nanocomposite hydrogels were synthesized by *in situ* free radical polymerization of AA and AM in the GQD dispersion. Typically, a certain amount of deionized water and GQDs was added, and the total volume of the dispersion was 5.0 mL. Afterwards, 1.0 mL of AA was neutralized to a neutralization degree of 30 mol% with 30 wt% NaOH solution in an ice bath. Subsequently, AM (2.5 g), APS (0.03 g) and TEMED (20 μL) were added to the system under stirring for 20 min, respectively. Finally, the dispersion was transferred to a sealed centrifugal tube and the polymerization was performed at 20 °C for 48 h. After polymerization, the as-prepared hydrogels were removed, cut into disks, and then soaked in a large amount of deionized water for 1 week. The water was exchanged daily to remove monomers and oligomers which were not incorporated into the gels. The poly(AM-*co*-AA)/GQD nanocomposite hydrogels were dried in an oven at 70 °C until a constant weight.

As a control, the linear neat poly(AM-*co*-AA) hydrogel was prepared according to an identical procedure to that above apart from GQDs.

Characterization

A Fourier transform infrared spectrometer (FTIR, Nicolet 6700, Thermo Fisher Scientific, USA) was used to record the vibration of the functional groups of GQDs and oven-dried hydrogels in the wavenumber range of 4000 to 400 cm^{-1}. Raman spectroscopy was performed from 500 to 2500 cm^{-1} at room temperature using a Raman spectrometer (Dxr2xi, Thermo Fisher Scientific, USA) with an incident laser at a wavelength of 532 nm. The HRTEM analysis of GQDs and oven-dried hydrogel was investigated by transmission electron microscopy (TEM, Tecnai G2 F20, FEI Company, USA) with an accelerating voltage of 200 kV. The GQDs and pre-prepared hydrogel/acetone dispersion were dropped onto copper wire mesh and dried at room temperature, then coated with gold prior to TEM analysis. The surface morphology of the GQDs was determined by atomic force microscopy (AFM, Hitachi High-Tech Science, E-SEEEP). The GQDs dispersion was dropped onto a mica sheet and dried at room temperature in advance. The SEM photographs of the hydrogels were observed using field emission scanning electron microscopy (FESEM, Apreo 2C, Thermo Fisher Scientific, USA) with an accelerating voltage of 10 kV. The samples were immersed in deionized water to reach equilibrium prior to freeze drying (FD-1C-50) for 48 h, then coated with gold before SEM analysis. X-ray diffraction (XRD) patterns were recorded by a D2 PHASER (Bruker, Germany) X-ray diffractometer (40 kV, 30 mA) and a curved graphite crystal monochromator with Cu Kα radiation at a scanning rate of 0.5° min^{-1}.

Optical measurements

The fluorescence of the GQD dispersion and poly(AM-*co*-AA)/GQD nanocomposite hydrogels was measured by a fluorescence spectrophotometer (PELS-55, PerkinElmer, USA) at a fixed excitation wavelength of 360 nm. The hydrogel precursor was transferred between two glass plates separated by a 1 mm thickness rubber spacer to prepare samples for optical testing. Then the hydrogel film was cut into slices of 12 mm × 20 mm and placed in a fluorimeter quartz cuvette for testing. The excitation wavelength of 360 nm was selected to monitor the emission spectrum. A UV-Vis spectrometer (UV-1600PC, Shanghai Xipu instrument co., Ltd, China) was used for recording the optical absorption spectra of the GQD dispersion. A laser scanning confocal microscope (LSM880, Zeiss, Germany) was used to contrast the photoluminescence phenomenon of each component in the hydrogels under irradiation at 405 nm.

Mechanical properties measurements

The compressive strength and cyclic compressive measurements were obtained on a cylindrical hybrid hydrogel (10 mm diameter × 6–10 mm length) using a static mechanical tester (CMT4503, Meitesi Industry Co. Ltd, China) under a load of 2 kN at room temperature. The tensile strength and cyclic tensile tests of the as-prepared hydrogel samples (4 mm diameter × 60 mm length) were carried out by using the above test system. The length of the sample between the jaws was about 20 mm, and the crosshead speed was 100 mm min^{-1}. All the samples were tested three times.

Self-healing test

Hydrogels with and without 0.01 wt% rhodamine B were prepared according to the procedure described previously. The cylindrical hydrogels were cut into two separate parts. Afterward, the two separated halves were slightly connected with each other and placed at room temperature. Finally, the self-healing process took place in a sealed chamber at room temperature over a period of time. After self-healing, the tensile properties were tested.

Results and discussion

Synthesis and characterization of poly(AM-*co*-AA)/GQD nanocomposite hydrogels

Herein, a fluorescent nanocomposite hydrogel poly(AM-*co*-AA)/GQDs with GQDs as the multifunctional crosslinker was

prepared. GQDs were successfully prepared by the pyrolysis of citric acid, and the average diameter of GQDs was 3.62 ± 0.3 nm according to TEM analysis (Fig. 1a and b). The HRTEM (Fig. 1a inset) clearly showed that the lattice spacing of GQDs was observed to be 0.26 nm, corresponding to the (100) facet of bulk graphite, indicating that the synthesized GQDs have good crystallinity.[48] The AFM images in Fig. S1 (ESI†) showed the topographic morphology of GQDs, and the heights of GQDs were primarily between 1.3 and 5.2 nm. The average height of GQDs was about 3.1 nm, and more than 50% of the GQDs are less than 2 nm in height, suggesting that most GQDs consist of 2–9 graphene layers. UV-Vis spectroscopy measurements of the GQD dispersion (1 wt%) showed a broad absorption band at 400–480 nm (Fig. 1c). In addition, the GQD dispersion showed strong blue fluorescence with an emission peak at 475 nm when excited at 360 nm. The obtained GQDs could be uniformly dispersed in aqueous solution for a long time even at a high concentration (above 7 wt%), which made it possible to obtain a uniform dispersion of GQDs and monomers by mixing (Fig. 1d). On this basis, monomer, initiator and catalyst were successively added to the above GQD dispersion to obtain a uniform dispersion (Fig. 1e), and then the poly(AM-*co*-AA)/GQD nanocomposite hydrogels were finally prepared by *in situ* free radical polymerization (Fig. 1f). Due to the fluorescence of GQDs, the prepared poly(AM-*co*-AA)/GQD nanocomposite hydrogels could present obvious blue fluorescence under ultraviolet lamp irradiation (λ = 365 nm) (Fig. 1g).

The FTIR characterization of GQDs, poly(AM-*co*-AA) and poly(AM-*co*-AA)/GQD hydrogels was carried out. As shown in Fig. 2a, the FTIR characterization of GQDs exhibited clear peaks at 3435, 1598 and 1396 cm^{-1}, which were attributed to the stretching vibrations of O–H bonds and asymmetric and symmetric stretching vibrations of the C–O–C group, respectively. In addition, the peak at 1077 cm^{-1} was assigned to C–O bonds. This indicated that the surface of the GQDs prepared by pyrolysis of citric acid contained a large amount of functional groups such as hydroxyl and carboxyl groups.[45,47,49] The FTIR spectrum of pure poly(AM-*co*-AA) hydrogel showed a series of characteristic bands at 3442 cm^{-1} (–OH stretching of AA and N–H stretching of AM), 2927 cm^{-1} ($-CH_2-$ stretching of AA and AM), 1639 cm^{-1} (–C═N– of AM) and 1451 cm^{-1} (symmetric stretching of –COO– in AA).[50,51] The FTIR spectrum of poly(AM-*co*-AA)/GQD nanocomposite hydrogels displayed similar peaks to poly(AM-*co*-AA) hydrogels. However, in the nanocomposite hydrogel, the stretching vibration peak of the carboxyl group O–H in the pure polymer (3442 cm^{-1}) moved to 3437 cm^{-1}, indicating a strong interaction between the oxygen-containing groups of GQDs and the amide and carboxyl groups of the polymer side chain. This interaction was due to hydrogen bonding between the carboxyl and amino group of the poly(AM-*Co*-AA) chain and the surface of GQDs.[51–54] Fig. S2 (ESI†) shows the Raman spectra of GQDs and poly(AM-*co*-AA)/GQD hydrogels. For GQDs, the characteristic peaks located at 1339.13 and 1562.28 cm^{-1} were respectively ascribed to the disordered D band and crystalline G band. The intensity ratio of the D and G band (I_D/I_G) was 1.11, indicating that GQDs possessed many defects on the surface and high disorder degree. No obvious characteristic peaks of GQDs were found

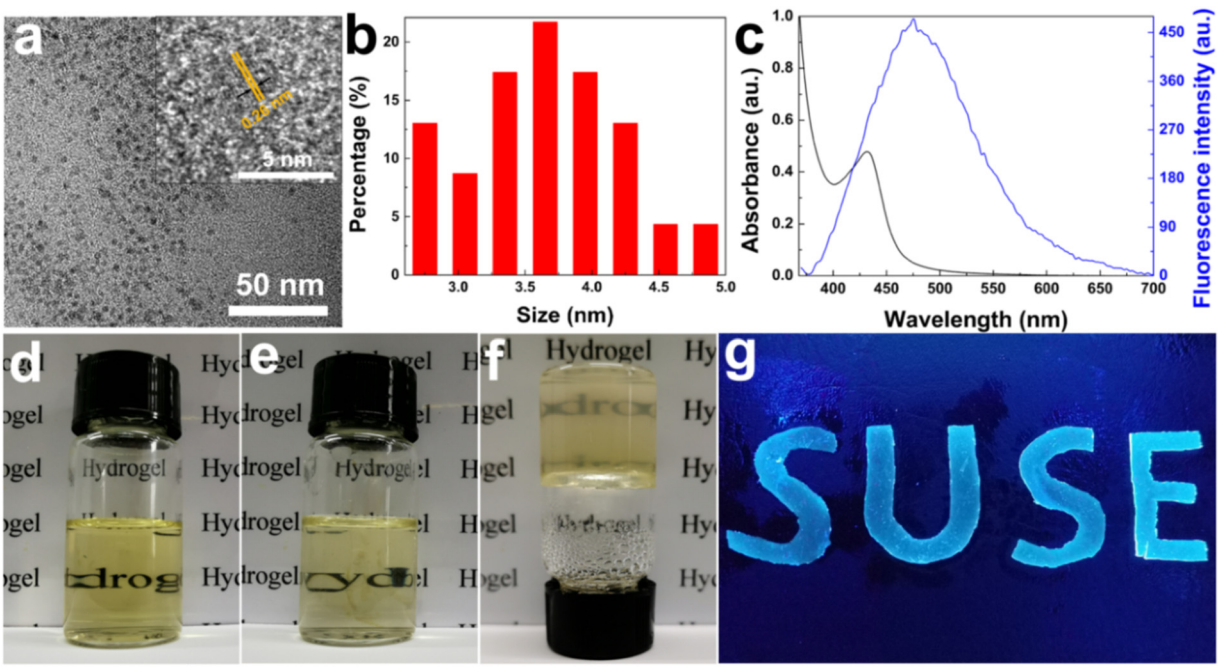

Fig. 1 (a) TEM image (inset: HRTEM image of GQDs showing lattice spacing), (b) size histogram (counting 100 particles at least), and (c) UV-Vis absorbance and fluorescence emission spectra of synthesised GQDs (1 wt%); preparation of poly(AM-*co*-AA)/GQD nanocomposite hydrogels ((d) optical images of an aqueous GQD dispersion, (e) GQD dispersion mixed with AM and AA, (f) nanocomposite hydrogels). (g) The obtained hydrogels exhibited obvious blue fluorescence under 365 nm UV light.

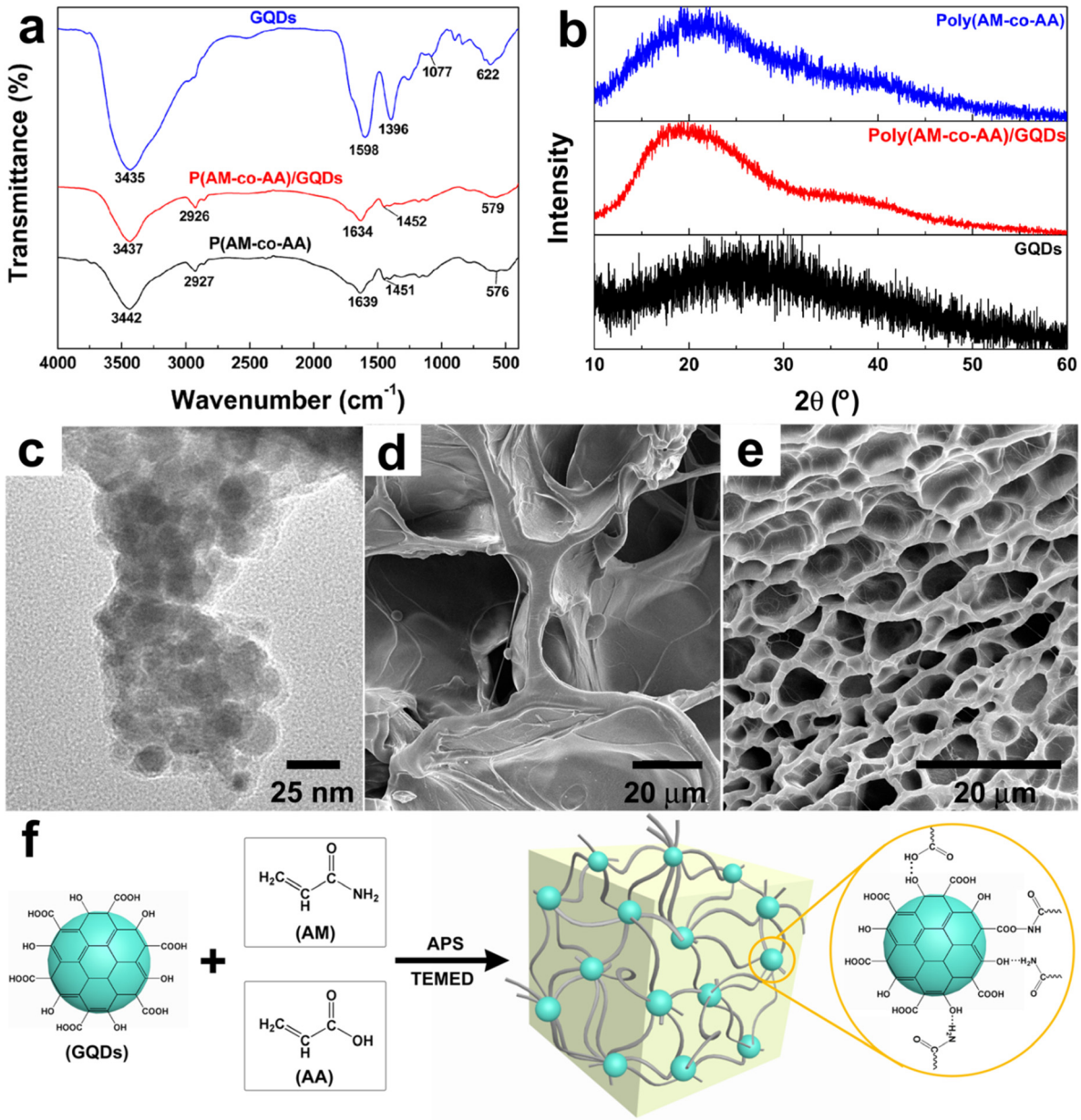

Fig. 2 (a) FTIR spectrum, (b) XRD patterns, and (c) TEM image of poly(AM-*co*-AA)/GQD nanocomposite hydrogels (1 wt% GQDs); (d and e) SEM photographs of poly(AM-*co*-AA) and poly(AM-*co*-AA)/GQD hydrogels (1 wt% GQDs), respectively; (f) schematic representation of the formation of poly(AM-*co*-AA)/GQD nanocomposite hydrogels and the supposed interactions between the polymer chains and the GQDs (enlarged drawing).

in poly(AM-*co*-AA)/GQD nanocomposite hydrogels due to the small amount of GQDs.

Fig. 2b shows the XRD patterns of GQDs, poly(AM-*co*-AA) and poly(AM-*co*-AA)/GQD hydrogels. The XRD patterns of GQDs showed a wide peak around 27.74°, indicating the existence of (002) planes of the graphitic structure.[55] The poly(AM-*co*-AA) hydrogels showed an obvious diffraction peak at 21.68°, which belonged to poly(AM-*co*-AA). The diffraction peak (19.74°) attributed to poly(AM-*co*-AA) could also be observed distinctly in poly(AM-*co*-AA)/GQD hydrogels. No diffraction peak of GQDs was found in poly(AM-*co*-AA)/GQD nanocomposite hydrogels due to the small amount of GQDs, which was consistent with the results in the Raman spectra. The TEM analysis of the hydrogel revealed the dispersion level of GQDs (Fig. 2c). Most of the GQDs were uniformly dispersed in the hydrogel matrix. In our work, GQDs were noncovalently bonded with the hydrogel matrix through free radical polymerization, so as to form an organic–inorganic nanocomposite network. That was the main reason for the greatly improved mechanical properties of the nanocomposite hydrogel.

The SEM images of the poly(AM-*co*-AA) and poly(AM-*co*-AA)/GQD hydrogels are presented in Fig. 2d and e, respectively. Both poly(AM-*co*-AA) and poly(AM-*co*-AA)/GQD hydrogels exhibited a honeycomb porous structure with interconnected pores. The difference is that the pore sizes became smaller and the pore walls became considerably thinner with the addition of

GQDs. This reconfirmed that the GQDs acted as multifunctional crosslinkers in gel networks with poly(AM-*co*-AA) chains, which made the crosslinking network more dense and thus reduced the pore sizes of the nanocomposite hydrogels. The relatively compact crosslinking density enabled the gel to dissipate stress more effectively when confronted with applied stress, which was conductive to improving the mechanical properties of poly(AM-*co*-AA)/GQD nanocomposite hydrogels. Furthermore, the highly porous structure was also beneficial to the diffusion of foreign ions into the gel matrix and making GQDs more fully in contact with Fe^{3+} in the solution. Therefore, this gel was suitable for flexible fluorescent probes.

Accordingly, the crosslinking mechanism of poly(AM-*co*-AA)/GQD nanocomposite hydrogels is proposed in Fig. 2f. During the polymerization process, the carboxyl and amino groups on the poly(AM-*co*-AA) chains were connected with GQDs through hydrogen bonds and formed a stable hydrogel with a three-dimensional network structure. This result could be further proven by the mechanical tests of hydrogels.

Mechanical performance of poly(AM-*co*-AA)/GQD nanocomposite hydrogels

The nanocomposite hydrogel had a strong mechanical strength and toughness, enough to remain intact under large deformation (compression to 90% of its original height), returning to its original size within a few seconds after unloading with almost no residual strain, indicating good toughness and fatigue resistance (Fig. 3a). In addition, the hydrogels could be severely knotted, cross-bended, and then stretched (Fig. 3b and c). This proved that the noncovalent bonds formed by GQD and poly(AM-*co*-AA) chains contributed greatly to the excellent mechanical properties of the hydrogels.

The effect of GQDs on the mechanical properties of hydrogel materials was studied by tensile and compression tests. As shown in Fig. 4a, the tensile properties of poly(AM-*co*-AA)/GQD hydrogels could be significantly improved by adding a small amount of GQDs. When 1 wt% GQDs was added, the fracture stress was up to 344.22 kPa and the corresponding elongation at break was 3437%, which were 4.04 and 4.51 times that of the poly(AM-*co*-AA) hydrogel, respectively. It was pointed out that GQDs doped in the poly(AM-*co*-AA) hydrogel network could act as a multifunctional crosslinker. Unfortunately, the increased content of GQDs reduced the tensile properties of the hydrogel. When the GQD content increased to 7 wt%, the tensile strength and elongation at break even decreased to 33.76 kPa and 66%, respectively. The addition of GQDs not only improved the tensile properties of the gel, but also greatly improved the compression properties of the hydrogel (Fig. 4b). When the tensile strain was fixed at 90%, the compressive strength of the poly(AM-*co*-AA)/GQD nanocomposite hydrogels with 1 wt% GQD content was up to 11.02 MPa, which was 1.06 times that of the pore poly(AM-*co*-AA) hydrogels. When the content of GQDs increased to 7 wt%, the compressive strength of the hydrogel was only 5.19 MPa, which was only half that of the poly(AM-*co*-AA) hydrogel, because the higher content of GQDs in the nanocomposite hydrogels tended to accumulate together and formed small aggregates. The small aggregates were not effective crosslinkers compared with the uniformly dispersed ones. This was why nanocomposite hydrogels with a high GQD content possessed lower mechanical properties. This conclusion is strongly consistent with the report of Xu *et al.*[56]

Surprisingly, the poly(AM-*co*-AA)/GQD nanocomposite hydrogels had excellent fatigue resistance. Fig. 4c shows the ten-time loading–unloading cyclic compression curves of the as-prepared nanocomposite hydrogels (1 wt% GQDs). It can be seen that the third to tenth measurements showed almost identical stress–strain behaviours to the second measurement cycle. Moreover, the loading–unloading cycle curves showed no obvious hysteresis loops. Meanwhile, the dissipated hysteresis energy and the compression stress at 85% strain during the cyclic loading–unloading process almost remained at 234.59 kJ m^{-3} and 5.55 MPa, respectively (Fig. 4d). These results indicated the excellent fatigue resistance of these nanocomposite hydrogels under compression loadings. This could be attributed to the nanocomposite structure which could dissipate energy effectively. As the loading was applied to the gel, the nanocomposite crosslinking structure could dissipate substantial mechanical energy but still maintain high elasticity under deformation effectively. Simultaneously, the effect of stress concentration was greatly weakened due to improved compatibility which was caused by the noncovalent bonds forming between GQDs and poly(AM-*co*-AA) chains, resulting in an improvement of the mechanical properties. Particularly, the excellent mechanical properties make the hydrogel suitable for flexible probes.

Fig. 3 The poly(AM-*co*-AA)/GQD hydrogels (1 wt% GQDs) exhibited significant mechanical toughness ((a) compressed and released, (b) cross-bent and stretched, and (c) knotted and stretched).

Self-healing performance of poly(AM-*co*-AA)/GQD nanocomposite hydrogels

The poly(AM-*co*-AA)/GQD nanocomposite hydrogels displayed a certain self-healing property. As shown in Fig. 5, the hydrogel sample was completely cut into two separate blocks with a blade, one of which was stained with rhodamine B (0.01 wt%) for observation, and then the two halves were brought into contact. After being sealed and stored in a glass desiccator for a certain period of time (10 h), the incisions were merged together at room temperature without any stimulation. The healed

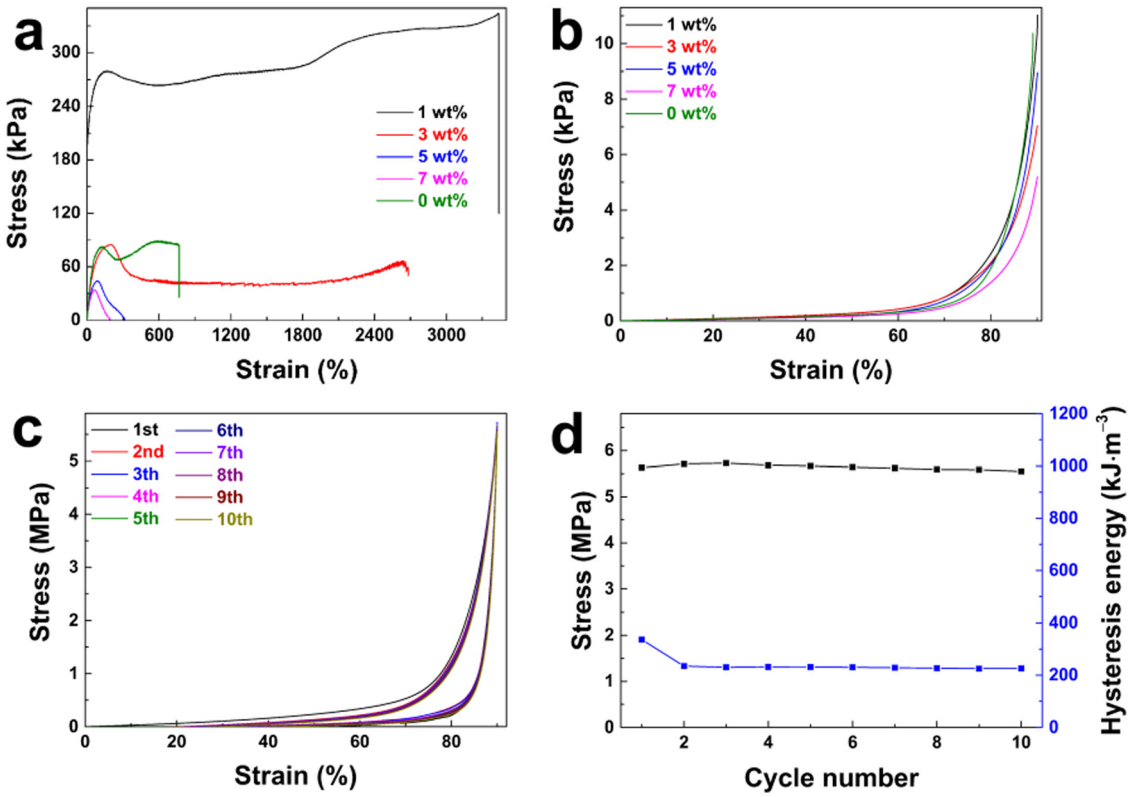

Fig. 4 Typical (a) tensile and (b) compressive stress–strain curves of the hydrogels with different GQD contents; (c) cyclic compression stress–strain curves, (d) stress-cycle number and hysteresis energy-cycle number curves of the hydrogel with 1 wt% GQDs at a fixed strain of 90%.

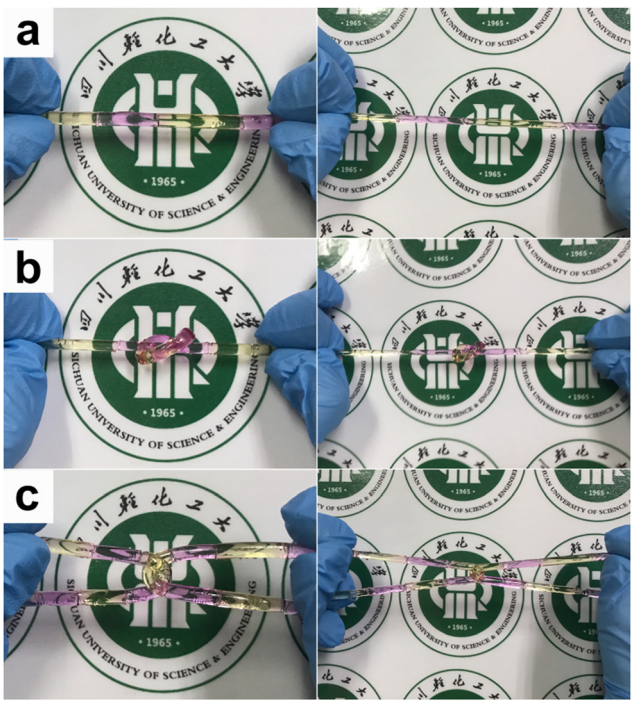

Fig. 5 Images showing the poly(AM-*co*-AA)/GQD nanocomposite gels (1 wt% GQDs) after being cut and then healed for 10 h. The healed sample could be (a) stretched, (b) knotted and stretched, and (c) cross-bent and stretched without breaking.

specimens could withstand knotting, cross-bending, and even stretching to a certain strain without fractures (Fig. 5a–c).

Fig. 6 shows the tensile test results for samples after a certain period of self-repair. It was found that the self-healing performance of the nanocomposite hydrogel could be significantly enhanced by prolonging the healing time. After 0.5 h of self-healing at room temperature, the fracture tensile strain of the hydrogel recovered by 0.79% and 5.38%, respectively.

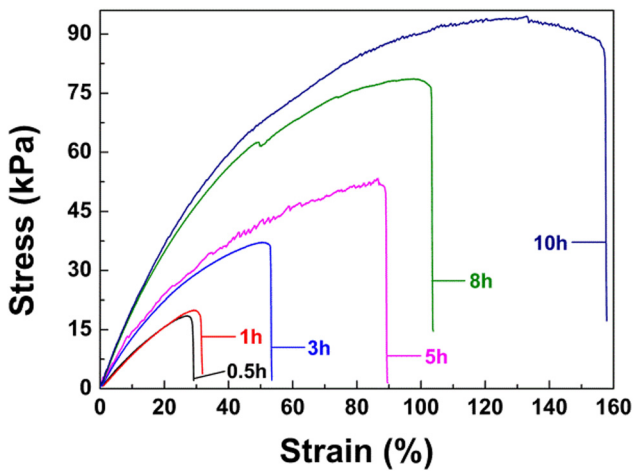

Fig. 6 Tensile stress–strain curves of the healed nanocomposite hydrogels with 1 wt% GQDs after different healing time.

Besides, the cut hydrogel could only recover 3.87% and 27.47% of the breaking tensile strain and stress after 10 h healing, respectively. It is well known that the self-healing properties of nanocomposite hydrogels are due to the strong and recoverable physical interaction between long flexible polymer chains and multifunctional cross-linkers. Therefore, the special, self-healing property of poly(AM-*co*-AA)/GQD nanocomposite hydrogels further confirmed the existence of strong noncovalent bonds between GQDs and poly(AM-*co*-AA) chains. Here, it should be noted that the self-healing efficiency of the hydrogels could not achieve 100% even after a much longer healing time due to the irreversible fracture of some polymer chains. The excellent self-healing ability can effectively prolong the service life of the hydrogel probe.

Fluorescence and sensing selectivity of the poly(AM-*co*-AA)/GQD nanocomposite hydrogel probe for Fe^{3+} ions

For the sensitivity study, different concentrations of Fe^{3+} in the range of 0–160 μmol L^{-1} were investigated. As shown in Fig. 7a, the addition of Fe^{3+} ions could quench the emission of poly(AM-*co*-AA)/GQD nanocomposite hydrogels. During the detection, Fe^{3+} in the aqueous solution penetrated into the hydrogel matrix through passive diffusion. Due to the strong coordination interaction between Fe^{3+} ions and carboxyl groups on the GQDs and poly(AM-*co*-AA) chains, which facilitated the non-radiative electron transfer from the GQD excited state to Fe^{3+} ions, the functional GQDs embedded in the hydrogel were quenched.[57] The fluorescence intensity of all the measured hydrogels at 459 nm gradually decreased with the increase of Fe^{3+} concentration. When the Fe^{3+} concentration was in the range of 10 μmol L^{-1} to 160 μmol L^{-1}, there was an approximately linear relationship between Fe^{3+} concentration and fluorescence intensity (R^2 = 0.9686) (Fig. 7b). Therefore, the gel material could be used as a fluorescent probe to indicate the concentration of Fe^{3+} in water within the concentration range.

Interestingly, poly(AM-*co*-AA)/GQD nanocomposite hydrogels showed an almost instantaneous response and maintained a deterioration in fluorescence once immersed in solutions of Fe^{3+} ions (Fig. 8a and b). The time-dependency of the fluorescence quenching was mainly attributed to diffusion of the Fe^{3+} into the hydrogel matrix. This rapid response was particularly

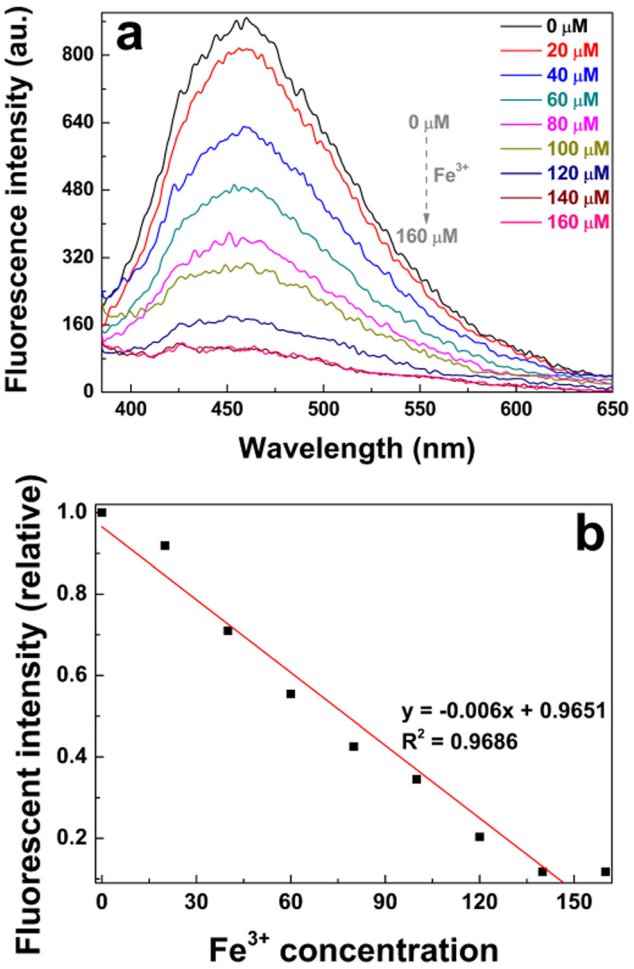

Fig. 7 (a) Fluorescence spectra and (b) the relationship between the fluorescence intensity of poly(AM-*co*-AA)/GQD nanocomposite hydrogels (1 wt% GQDs) and the concentration of Fe^{3+}.

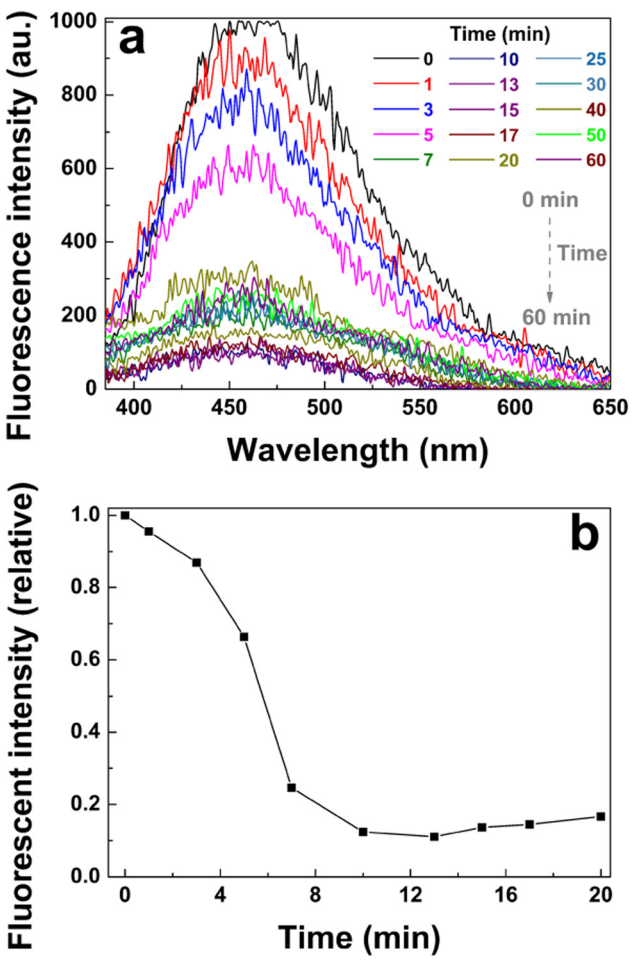

Fig. 8 Response time of the poly(AM-*co*-AA)/GQD nanocomposite hydrogels (1 wt% GQDs): (a) fluorescence spectra and (b) corresponding relative fluorescence intensity.

beneficial to the application of the poly(AM-*co*-AA)/GQD nanocomposite hydrogels in the field of fluorescent probes.

To further assess the selectivity of the poly(AM-*co*-AA)/GQD nanocomposite hydrogels to various metal ions, the fluorescence measurement was carried out after the samples were immersed in $BaCl_2$, $CaCl_2$, $CrCl_3$, $FeCl_3$, $CuSO_4$, $MgSO_4$, $Ni(NO_3)_2$, $Pb(NO_3)_2$ and $Zn(NO_3)_2$ solutions for 30 min, respectively. The concentration of each metal ion was kept at 100 μmol L^{-1}. The fluorescence response of the nanocomposite hydrogel to different metal ions is shown in Fig. 9a and b. As expected, the fluorescence of the nanocomposite hydrogel was significantly quenched by Fe^{3+} ions, and its relative intensity decreased to 0.35, demonstrating that our hydrogels were highly selective for Fe^{3+} detection. In addition, the nanocomposite gel had a certain quenching effect on Mg^{2+} and Cr^{3+}, and the relative fluorescence intensity of the hydrogels in Mg^{2+} and Cr^{3+} solutions was reduced to 0.42 and 0.48, respectively. This indicated that the gel could also serve as an effective sensor to detect these metal ions in the future. Additionally, as other species containing chloride ions *e.g.* $CaCl_2$ and $BaCl_2$, had no significant effect on the fluorescence of the nanocomposite hydrogel, the fluorescence reduction in the solution of $FeCl_3$ was attributed to the Fe^{3+} and not Cl^-.

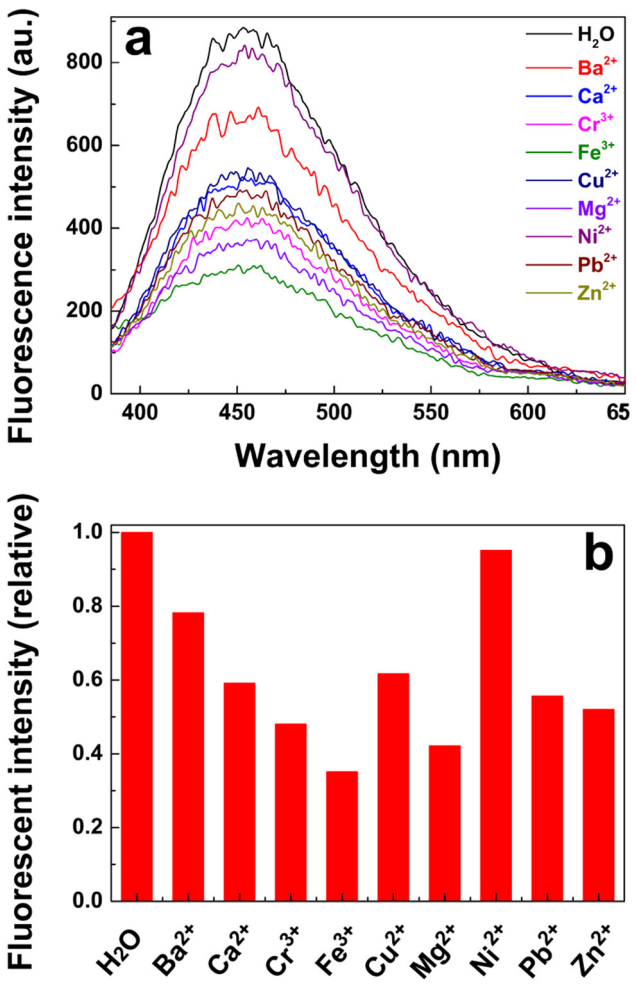

Fig. 9 Fluorescence response of the poly(AM-*co*-AA)/GQD nanocomposite hydrogels (1 wt% GQDs) to different ions dissolved in deionized water: (a) fluorescence spectra and (b) corresponding relative fluorescence intensity.

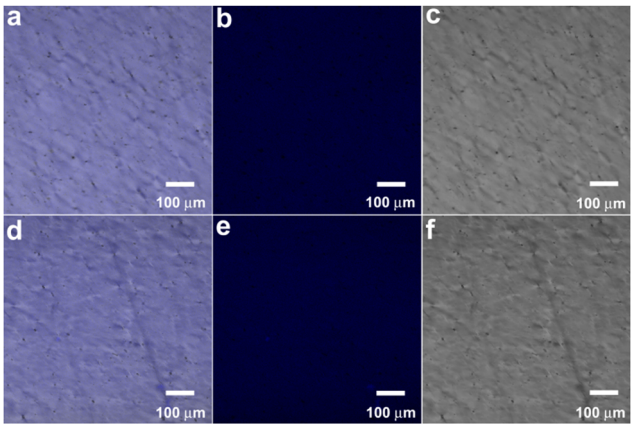

Fig. 10 Fluorescence images of poly(AM-*co*-AA)/GQD nanocomposite hydrogels (1 wt% GQDs) under irradiation at 405 nm ((a–c) without and (d–f) 30 min after $FeCl_3$ was added). (a and d) The images after superposition of both light field and dark field. (b, e and d, f) Images of the light field and dark field, respectively.

To examine the fluorescence properties of the gel in more detail, confocal microscopy was used to determine the distribution of GQDs in the nanocomposite hydrogel and to monitor its fluorescence changes when exposed to $FeCl_3$ solution. Confocal imaging showed that GQDs were evenly distributed in poly(AM-*co*-AA)/GQD hydrogels (Fig. 10a–c). This was consistent with the results of TEM. Meanwhile, time-lapse fluorescence images were recorded to investigate the influence of Fe^{3+} on the fluorescence of the poly(AM-*co*-AA)/GQD hydrogels. The results in Fig. 10d–f show that after adding $FeCl_3$ solution, the dissolved Fe^{3+} was rapidly absorbed by poly(AM-*co*-AA)/GQD nanocomposite hydrogels, and the fluorescence was significantly reduced.

Conclusions

In summary, we successfully demonstrated fluorescent nanocomposite hydrogel poly(AM-*co*-AA)/GQDs through *in situ* free radical polymerization of AM and AA monomers in an aqueous dispersion of GQDs. The test results of TEM, FTIR and XRD indicated that the appropriate size of GQDs and the strong hydrogen-bond interaction between poly(AM-*co*-AA) chains and GQDs made GQDs a multifunctional crosslinker for poly(AM-*co*-AA)/GQD nanocomposite hydrogels. As a result, the prepared poly(AM-*co*-AA)/GQD nanocomposite hydrogels showed excellent mechanical toughness, fatigue resistance, and self-healing properties. Compared to poly(AM-*co*-AA) hydrogels, about a 4.04-fold increase of tensile strength, a 4.51-fold increase of elongation at break and 1.06 times compressive strength compared to those of poly(AM-*co*-AA) hydrogels were achieved when the content of GQDs in the poly(AM-*co*-AA)/GQD nanocomposite hydrogels was 1 wt%. Moreover, GQDs provided

excitation-dependent fluorescence properties to the poly(AM-*co*-AA)/GQD nanocomposite hydrogels. The hydrogels had selectivity to Fe^{3+} ions and possessed a fast and continuously linear response to Fe^{3+} ions in the concentration range of 10–160 μmol L^{-1} (R^2 = 0.9686). All the results indicated strong prospects for the use of the poly(AM-*co*-AA)/GQD hydrogels in a deployable sensor for the detection of aqueous Fe^{3+} contamination in water.

Conflicts of interest

There are no conflicts to declare.

Acknowledgements

The work was supported by the Sichuan Science and Technology Program (No. 2022JDRC0090) and the Opening Project of Material Corrosion and Protection Key Laboratory of Sichuan Province, China (No. 2020CL21 and 2020CL22).

Notes and references

1 P. T. Lieu, M. Heiskala, P. A. Peterson and Y. Yang, *Mol. Aspects Med.*, 2001, **22**, 1–87.
2 S. V. Torti and F. M. Torti, *Nat. Rev. Cancer*, 2013, **13**, 342–355.
3 D. Galaris, V. Skiada and A. Barbouti, *Cancer Lett.*, 2008, **266**, 21–29.
4 L. Yu, M. He, S. Liu, X. Dou, L. Li, N. Gu, B. Li, Z. Liu, G. Wang and J. Fan, *ACS Appl. Mater. Interfaces*, 2021, **13**, 54677–54689.
5 C. Zhang, Y. Cui, L. Song, X. Liu and Z. Hu, *Talanta*, 2016, **150**, 54–60.
6 A. A. Belaidi and A. I. Bush, *J. Neurochem.*, 2016, **139**, 179–197.
7 G. A. Antunes, H. S. dos Santos, Y. P. da Silva, M. M. Silva, C. M. S. Piatnicki and D. Samios, *Energy Fuels*, 2017, **31**, 2944–2950.
8 D. V. Biller and K. W. Bruland, *Mar. Chem.*, 2012, **130-131**, 12–20.
9 Y. Zhu, D. Pan, X. Hu, H. Han, M. Lin and C. Wang, *Sens. Actuators, B*, 2017, **243**, 1–7.
10 L. Zhao, F. Geng, F. Di, L.-H. Guo, B. Wan, Y. Yang, H. Zhang and G. Sun, *RSC Adv.*, 2014, **4**, 45768–45771.
11 B. Peng, Y. Shen, Z. Gao, M. Zhou, Y. Ma and S. Zhao, *Food Chem.*, 2015, **176**, 288–293.
12 O. Sadak, A. K. Sundramoorthy and S. Gunasekaran, *Biosens. Bioelectron.*, 2017, **89**, 430–436.
13 A. Ibarbia, L. Sánchez-Abella, L. Lezama, H. J. Grande and V. Ruiz, *Appl. Surf. Sci.*, 2020, **527**, 146937.
14 S. Javanbakht and H. Namazi, *Mater. Sci. Eng., C*, 2018, **87**, 50–59.
15 V. M. Naik, D. B. Gunjal, A. H. Gore, P. V. Anbhule, D. Sohn, S. V. Bhosale and G. B. Kolekar, *Anal. Bioanal. Chem.*, 2020, **412**, 2993–3003.
16 T. V. Tam, N. B. Trung, H. R. Kim, J. S. Chung and W. M. Choi, *Sens. Actuators, B*, 2014, **202**, 568–573.
17 M. Hu, Y. Yang, X. Gu, Y. Hu, Z. Du and C. Wang, *Macromol. Mater. Eng.*, 2015, **300**, 1043–1048.
18 A. Cayuela, M. L. Soriano, S. R. Kennedy, J. W. Steed and M. Valcárcel, *Talanta*, 2016, **151**, 100–105.
19 R. Suntornnond, E. Y. S. Tan, J. An and C. K. Chua, *Sci. Rep.*, 2017, **7**, 16902.
20 J. Li and D. J. Mooney, *Nat. Rev. Mater.*, 2016, **1**, 16071.
21 J. A. Hunt, R. Chen, T. van Veen and N. Bryan, *J. Mater. Chem. B*, 2014, **2**, 5319–5338.
22 E. Caló and V. V. Khutoryanskiy, *Eur. Polym. J.*, 2015, **65**, 252–267.
23 Y. Yin, C. Wu, J. Wang, F. Song, W. Yue and W. Zhong, *Chem. Commun.*, 2017, **53**, 529–532.
24 I. Y. Jung, J. S. Kim, B. R. Choi, K. Lee and H. Lee, *Adv. Healthcare Mater.*, 2017, **6**, 1601475.
25 Y. Okumura and K. Ito, *Adv. Mater.*, 2001, **13**, 485–487.
26 J. P. Gong, *Soft Matter*, 2010, **6**, 2583–2590.
27 K. Haraguchi and T. Takehisa, *Adv. Mater.*, 2002, **14**, 1120–1124.
28 T. Huang, H. G. Xu, K. X. Jiao, L. P. Zhu, H. R. Brown and H. L. Wang, *Adv. Mater.*, 2007, **19**, 1622–1626.
29 Y. Tan, R. Wu, H. Li, W. Ren, J. Du, S. Xu and J. Wang, *J. Mater. Chem. B*, 2015, **3**, 4426–4430.
30 G. Gao, Z. Wang, D. Xu, L. Wang, T. Xu, H. Zhang, J. Chen and J. Fu, *ACS Appl. Mater. Interfaces*, 2018, **10**, 41724–41731.
31 S. Chatterjee, M. W. Lee and S. H. Woo, *Carbon*, 2009, **47**, 2933–2936.
32 K. Haraguchi, H.-J. Li, Y. Xu and G. Li, *Polymer*, 2016, **96**, 94–103.
33 D. Wang, Y. Tan, H. Xu, X. Wang, L. Yu, Z. Xiao, J. Wang and S. Xu, *Appl. Surf. Sci.*, 2019, **467-468**, 588–595.
34 J. Ling, N. Li, X. Yang, J. Ma, J. Du, D. Wang, Y. Tan, F. Yue and S. Xu, *J. Appl. Polym. Sci.*, 2017, 134.
35 J. Y. Kim, Y. Choi, J. Choi, Y.-J. Kim, J. Kang, J. P. Kim, J. H. Kim, O. Kwon, S.-S. Kim and D. W. Kim, *ACS Appl. Mater. Interfaces*, 2022, **14**, 11779–11788.
36 P. Thoniyot, M. J. Tan, A. A. Karim, D. J. Young and X. J. Loh, *Adv. Sci.*, 2015, **2**, 1400010.
37 B. Xu, H. Li, Y. Wang, G. Zhang and Q. Zhang, *Polym. Compos.*, 2016, **37**, 810–817.
38 Z. Zhou, C. Qian and W. Yuan, *Compos. Sci. Technol.*, 2021, **203**, 108608.
39 D. Zhang, J. Yang, S. Bao, Q. Wu and Q. Wang, *Sci. Rep.*, 2013, **3**, 1399.
40 Y. Yang, Y. Tan, X. Wang, W. An, S. Xu, W. Liao and Y. Z. Wang, *ACS Appl. Mater. Interfaces*, 2018, **10**, 7688–7692.
41 C. H. Zhu, Z. B. Hai, C. H. Cui, H. H. Li, J. F. Chen and S. H. Yu, *Small*, 2012, **8**, 930–936.
42 Y. Ohm, C. Pan, M. J. Ford, X. Huang, J. Liao and C. Majidi, *Nat. Electron.*, 2021, **4**, 185–192.
43 Z. Zhang, Z. Yao, Y. Li, S. Lu, X. Wu and Z. Jiang, *Chem. Eng. J.*, 2022, **433**, 134488.
44 Y. Feng, H. Liu, W. Zhu, L. Guan, X. Yang, A. V. Zvyagin, Y. Zhao, C. Shen, B. Yang and Q. Lin, *Adv. Funct. Mater.*, 2021, **31**, 2105264.
45 D. W. M. Pincher, C. A. Bader, J. D. Hayball, S. E. Plush and M. J. Sweetman, *ChemistrySelect*, 2019, **4**, 9640–9646.

46 M. Hu, X. Gu, Y. Hu, Y. Deng and C. Wang, *Macromol. Mater. Eng.*, 2016, **301**, 1352–1362.
47 T. Alizadeh and M. Shokri, *Sens. Actuators, B*, 2016, **222**, 728–734.
48 T. V. Tam, S. H. Hur, J. S. Chung and W. M. Choi, *Sens. Actuators, B*, 2021, **329**, 129250.
49 M. Hu, Y. Yang, X. Gu, Y. Hu, J. Huang and C. Wang, *RSC Adv.*, 2014, **4**, 62446–62452.
50 H. Mittal, S. B. Mishra, A. K. Mishra, B. S. Kaith, R. Jindal and S. Kalia, *Carbohydr. Polym.*, 2013, **98**, 397–404.
51 B. Xu, H. Li, Y. Wang, G. Zhang and Q. Zhang, *RSC Adv.*, 2013, **3**, 7233–7236.
52 R. E. Tanner, Y. Liang and E. I. Altman, *Surf. Sci.*, 2002, **506**, 251–271.
53 R. E. Tanner, A. Sasahara, Y. Liang, E. I. Altman and H. Onishi, *J. Phys. Chem. B*, 2002, **106**, 8211–8222.
54 Y. X. Weng, L. Li, Y. Liu, L. Wang and G. Z. Yang, *J. Phys. Chem. B*, 2003, **107**, 4356–4363.
55 S. Nayak, S. R. Prasad, D. Mandal and P. Das, *J. Hazard. Mater.*, 2020, **392**, 122287.
56 J. Du, D. Wang, S. Xu, J. Wang, Y. Liu and J. Huang, *Appl. Clay Sci.*, 2017, **150**, 71–80.
57 M. Zhou, J. Guo and C. Yang, *Sens. Actuators, B*, 2018, **264**, 52–58.